DESIGN AND PERFORMANCE OF THE BEAMLET AMPLIFIERS

A. C. Erlandson

M. D. Rotter

D. N. Frank

R. W. McCracken

Introduction

In future laser systems, such as the National Ignition Facility (NIF), multi-segment amplifiers (MSAs) will be used to amplify the laser beam to the required levels. As a prototype of such a laser architecture, we have designed, built, and tested flash-lamp-pumped, Nd:Glass, Brewster-angle slab MSAs for the Beamlet project.

In this article, we review the fundamentals of Nd:Glass amplifiers, describe the MSA geometry, discuss parameters that are important in amplifier design, and present our results on the characterization of the Beamlet MSAs. In particular, gain and beam steering measurements show that the Beamlet amplifiers meet all optical performance specifications and perform close to model predictions.

The Beamlet amplifiers also demonstrate advances in MSA mechanical design: hermetically sealed blast shields to protect the laser slabs from contamination generated by the flash lamps; hermetically sealed flash-lamp cassettes to protect the lamp envelopes from outside sources of contamination; modular slab cassettes to reduce the size of the amplifier parts that need to be handled; and flash-lamp cassettes that can be installed and removed without disturbing the laser slabs. These features will be included in the amplifiers for the NIF.

Background

The Amplifier Pumping Process

Many energy transfer steps occur during the amplifier pumping process,[1] which begins when the switch in the flash-lamp discharge circuit is closed and current begins to flow through the flash lamps. Typically, circuits transfer 70–90% of the bank energy to the flash lamps, with the remainder lost as heat to the circuit elements. Flash-lamp plasmas convert about 80% of the delivered electrical energy to photons, with approximately half the optical output energy falling in the 400–1000-nm region of Nd^{3+} pumping bands. As these photons circulate in the pump cavity, some are reabsorbed by the flash-lamp plasma, which in turn re-emits a fraction of this reabsorbed energy; some are absorbed by the metal reflectors or slab holders; and some are lost through the ends of the amplifiers. The remaining photons (about 10% of those emitted by the plasma) are absorbed by the laser slabs.

The photons absorbed by the laser slabs produce stored energy in the form of excited Nd^{3+} ions. However, due to quantum defects between the absorbed photons and the upper laser level, about half of the absorbed energy is immediately converted to heat, depending on the spectral distribution of the flash-lamp light. Energy transfer from excited ions to ground-state ions (concentration quenching) produces additional heating.

Pump-induced beam steering and wavefront distortion arise from two main sources: (1) The laser slabs are warped when pump light deposits more heat on one side than the other. This warping causes beam steering and wavefront distortion that is distributed over the entire aperture. (2) Amplified spontaneous emission (ASE) heats the absorbing edge claddings that are used to prevent parasitics. The resulting thermal expansion produces significant wavefront distortion within approximately one slab thickness of the edge claddings. This edge distortion can be avoided by setting the beam aperture appropriately.

UCRL-LR-105821-95-1

Parameters Governing Amplifier Performance

In Brewster-angle slab amplifiers, the three most important parameters for describing laser performance are α, the average gain coefficient; g, the small signal gain per slab; and a, the hard aperture area. Both α and g are related to the stored energy density, ρ, by the relations

$$\alpha = \sigma\rho / h\nu \quad (1)$$

and

$$g = \exp\left[\alpha\left(n^2+1\right)^{1/2}(t/n)\right] \quad , \quad (2)$$

where σ is the stimulated emission cross section for excited Nd ions, $h\nu$ is the laser photon energy, n is the refractive index of the laser glass, and t is the caliper thickness of the laser glass. The term $(n^2+1)^{1/2}(t/n)$ is the beam path length through the Brewster-angle laser slab.

Generally, high values of α, g, and a are desired: as α increases, the desired beam fluence is achieved with less laser glass and, as a result, with smaller nonlinear phase shifts; as g increases, the desired fluence is achieved with fewer slabs; and as a increases, the desired laser energy can be achieved with fewer beamlets. However, it is difficult to attain the desired values for all three key amplifier performance parameters simultaneously. For example, increased ASE causes both α and g to decrease as a is increased. The gain per slab can be increased by making slabs thicker, but, as a result, α falls because flash-lamp light is preferentially absorbed near the slab surfaces. The sophisticated amplifier model[2] that Lawrence Livermore National Laboratory (LLNL) has developed to predict α and g is essential for characterizing tradeoffs between parameters and for arriving at cost-effective fusion laser designs.

Other important amplifier parameters are gain uniformity across the aperture, pump-induced wavefront distortion, and storage efficiency. A measure of gain uniformity is the parameter U, defined as the peak-to-average ratio of the gain coefficient evaluated over the beam aperture. Good gain uniformity, i.e., U close to unity, is desired because gain variations produce fluence variations in the output beam, thereby reducing the damage-limited output energy. Low pump-induced wavefront distortion is desired for good beam focusability and high harmonic-conversion efficiency. To some degree, both gain variations and pump-induced wavefront distortion can be compensated for, albeit at additional cost and complexity to the system. For example, the Beamlet preamplifier section uses a variable transmission filter to tailor the fluence distribution and a deformable mirror to precorrect the wavefront. To evaluate pump cavity designs, models for predicting gain distributions[3] and pump-induced wavefront distortion[4] are being developed at LLNL and at the CEA Laboratory in Limeil, France.

Storage efficiency, η, is defined as the total extractable energy stored in the laser slabs divided by the total electrical energy delivered to the flash lamps. High storage efficiency is desired to reduce the size and therefore cost of the pulsed power system.

Multisegment Amplifier (MSA) Development

Prior to Beamlet, all flash-lamp-pumped Nd:Glass fusion lasers have used one-beam-per-box amplifiers. MSAs, in which several beams are contained in the same amplifier box, were first proposed in 1978 as a way to reduce the cost of flash-lamp-pumped, Nd:Glass fusion laser systems.[5] MSAs cost less than the one-beam-per-box amplifiers in three ways: (1) by making amplifiers more compact, thereby reducing the size and cost of the building; (2) by increasing pumping efficiency, thereby reducing the size and cost of the pulsed power system; and (3) by reducing the number of internal amplifier parts.

Figure 1 shows the MSA design currently envisioned for the NIF. Optical gain at the 1.05-μm wavelength is provided by Nd-doped, phosphate glass, rectangular laser slabs oriented at Brewster's angle with respect to the beam to eliminate reflection losses. The amplifier hard apertures are 40×40 cm^2. The slabs are stacked four-high in holders that are arranged in 12 columns.

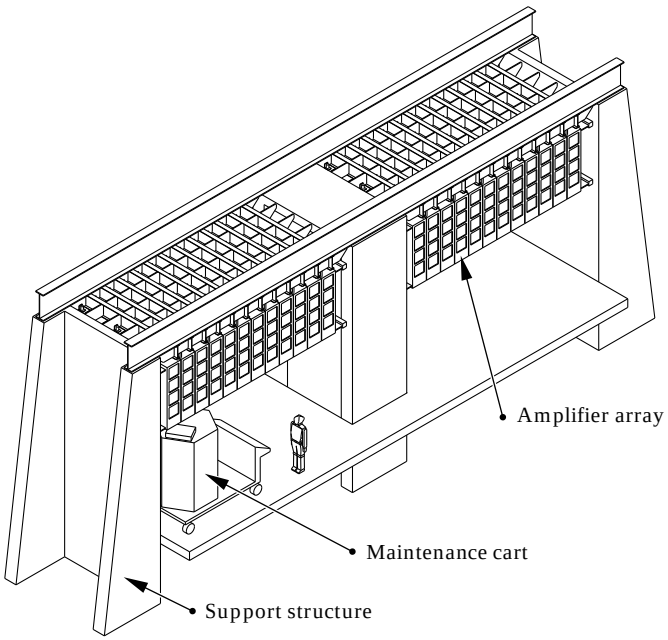

FIGURE 1. The MSA design currently envisioned for the NIF uses 48 apertures arranged in a 4-slab-high × 12-slab-wide matrix. (40-00-0294-0535pb01)

The columns of slabs are separated by arrays of central flash lamps that emit radiation to both sides. The outermost columns are also illuminated by arrays of side flash lamps that have large silver reflectors to redirect the flash-lamp radiation toward the slabs. In this respect, the side flash-lamp arrays are similar to the arrays used in one-beam-per-box amplifiers on Nova and other previous fusion lasers. Glass blast shields, placed between the flash lamps and the laser slabs, serve two purposes: (1) They prevent acoustic waves generated by the flash lamps from propagating into the beam path and causing wavefront distortion; and (2) they provide a contamination barrier between the flash-lamp cavity and the critical slab cavity. The blast shields also form a channel that could potentially be used for flowing cooling gas around the flash lamps. To simplify assembly and maintenance, the NIF MSAs would be assembled from one-slab-long, one-slab-wide, four-slab-high modules. In addition, the flash lamps would be mounted in 6- or 8-lamp removable cassettes.

Since 1989, LLNL has built and tested three MSA designs: MSA-1[2], MSA-2[6], and the Beamlet amplifiers. Although MSA-1 and MSA-2 contained only four apertures, in a one-slab-long, 2×2 array, they were large enough to permit us to study important MSA performance issues. In particular, we discovered that central flash-lamp arrays pump more efficiently than side flash-lamp arrays. In side arrays, the large reflectors return a portion of the flash-lamp radiation to the lamps, where it is absorbed by the plasma. Furthermore, the reflectors themselves absorb a significant fraction of the flash-lamp radiation. In contrast, central flash-lamp arrays allow the lamps to radiate freely in both directions, and the only reflectors are small diamond-shaped reflectors between the lamps that effectively reduce the transfer of radiation from lamp to lamp. Although MSA-1 had high storage efficiency (about 3.5%) and high average gain coefficient (5.5%/cm) at the normal operating point (lamps fired at 20% of the single-shot explosion energy), gain varied significantly across its aperture. MSA-1 was not versatile enough to permit us to explore solutions to the gain uniformity problem or to study how MSA performance is affected by changes in pump cavity design.

MSA-2, also called the Beamlet prototype amplifier, was used to develop pump cavity designs for the Beamlet amplifiers. MSA-2 had a flexible pump cavity that enabled us to study the effect of different designs on gain uniformity and cavity transfer efficiency. Gain gradients in the vertical direction were reduced by installing reflectors at the tops and bottoms of the flash-lamp cassettes to reduce the loss of pump radiation through the gaps between the flash lamps, and by installing dimpled silver reflectors with raised surfaces on the slab holders so that the reflected light illuminated the facing slabs more uniformly. Gain gradients in the horizontal direction were reduced by replacing the cylindrical silver reflectors in the side lamp arrays with flat reflectors. These changes lead to an extremely uniform gain distribution, with a gain uniformity parameter $U = 1.025 \pm 0.004$. Pumping was balanced between the 12-lamp central array and the less efficient side arrays by increasing the number of lamps in the side arrays from six to eight. Balanced pumping is desired to reduce wavefront distortions caused by slab warping due to preferential heating of one side of the laser slab by pump radiation.

Beamlet Amplifiers

Although testing MSA-1 and MSA-2 greatly enhanced our understanding of MSA performance, their 29×29 cm^2 apertures had only about 50% of the area of the 40×40 cm^2 apertures proposed for the NIF, and serious concerns remained regarding the feasibility of manufacturing large laser slabs and the effect of increased ASE on efficiency and gain uniformity. In addition, it remained to be demonstrated that MSAs could be cleanly assembled and operated. These issues were addressed by designing, building, and testing the Beamlet amplifiers.

Amplifier Description

The Beamlet amplifiers use the MSA architecture in which four apertures are arranged in a 2×2 matrix. Figure 2(a) shows an assembled Beamlet amplifier, with one end open. Beamlet contains two large amplifiers: a four-pass, eleven-slab-long cavity amplifier and a singlepass, five-slab-long booster amplifier. The positions of these amplifiers in the laser chain are discussed in "System Description and Initial Performance Results for Beamlet," p 1. The hard apertures of the Beamlet amplifiers are 39.5×39.5 cm^2, larger than the apertures used for any previous Nd:Glass amplifiers and approximately the same size as the amplifiers envisioned for the NIF.

The measurements described below show that at the standard operating point, for which the lamps are driven at 20% of their single-shot explosion energy (in air), the amplifiers have the following characteristics: the average gain coefficient is 5%/cm, the storage efficiency is 3%, and pump-induced wavefront distortion is <1.5 waves at 1.053 μm for the entire system. The ratio of peak gain coefficient to average gain coefficient, evaluated over the central 95% of the amplifier hard aperture, is 1.06:1. The gain distribution is influenced by ASE, which preferentially depumps the edges of the aperture.

The Beamlet amplifiers were designed modular, which facilitates assembly and maintenance. The basic amplifier assembly units (BAUs) are one slab long, one slab wide, and two slabs high. Each BAU consists of an aluminum frame, blast shields mounted on the sides, and a slab

holder mounted internally, as shown in Fig. 2(b). The aluminum frame is nickel-plated, for cleanliness. The BAUs are assembled in a class-100 clean room, bagged, and transported to the laser bay. In the laser bay, a crane lifts the BAUs onto rails, which allows the BAUs to be easily positioned along the direction of the laser beam. The BAUs are installed in pairs and bolted together side by side to form one-slab-long 2×2 units. The flash-lamp cassettes are slid into place from the top, using the crane. All amplifier assembly is performed under portable class-100 clean rooms.

The laser slabs are made of Schott glass (composition LG-750), doped at a Nd ion concentration of 3.5×10^{20} ions/cm^3. The finished slab dimensions are $4 \times 42.4 \times 76.4$ cm^3, excluding the 1.2-cm-thick edge claddings glued onto the perimeter to absorb ASE. The edge claddings are made of Cu-doped LG-750, which has an absorption coefficient of 2.8/cm at the peak gain wavelength of 1.053 μm. The volume of the Beamlet laser slabs is 12 L, nearly twice the volume of the largest laser slabs fabricated previously. Further details about the laser slabs are contained in the article "Large-Aperture, High-Damage-Threshold Optics for Beamlet," p. 52.

To reduce costs, only one of the four Beamlet apertures has real laser slabs. The other three apertures have dummy slabs consisting of two panes of Greylight-14, a relatively inexpensive architectural glass. These dummy slabs are indistinguishable from the real laser slabs in the degree to which they absorb flash-lamp light. The pumped regions of the slabs measure 39.5×75.6 cm^2. The vertical separation between the hard apertures is 5.5 cm. Like MSA-2, the slab masks use dimpled, silver reflectors, to improve gain uniformity.

Figure 3 shows a plan view of the pump cavity, the design of which is based on the MSA-2 results. The bore diameter of the flash lamps is 2.5 cm and the arc length is 91.4 cm. The flash lamps are made of UV-absorbing Ce-doped quartz to protect the pump

(a)

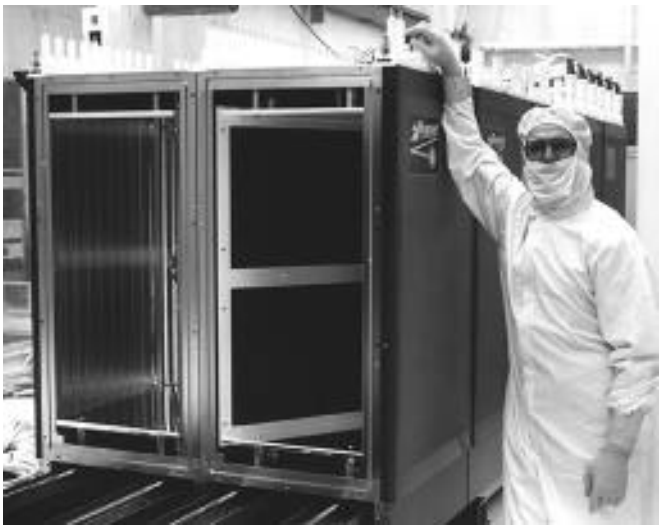

(b)

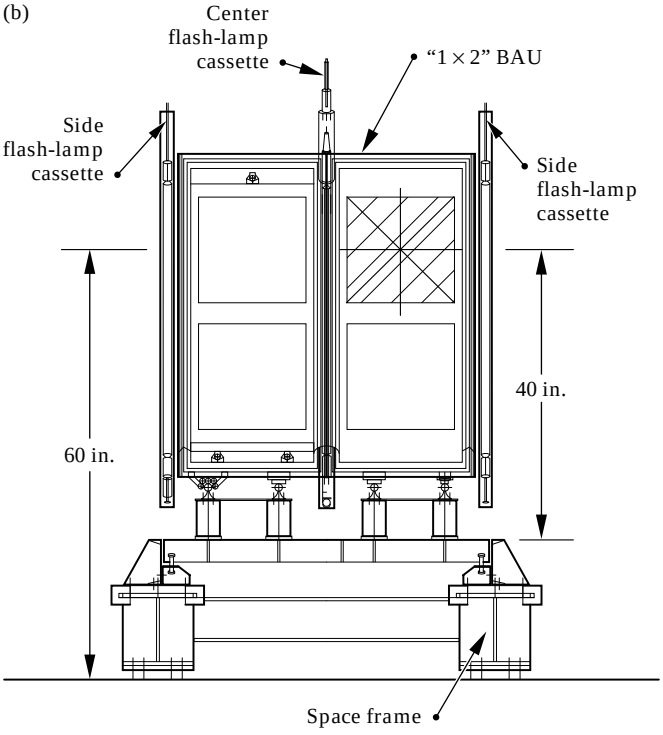

FIGURE 2. (a) Photograph of assembled 2×2 Beamlet amplifiers with 39.5×39.5 cm^2, hard-edged apertures (this supports about a 35×35 cm^2 beam size). (b) Schematic drawing showing key elements of the design: the shaded square represents the active beam aperture. (02-30-1093-3491Apb01)

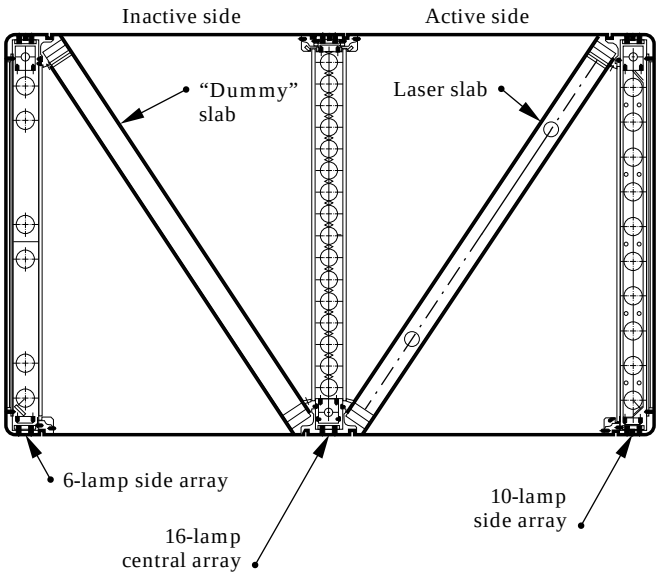

FIGURE 3. Plan view of the Beamlet pump cavity showing flash-lamp and slab locations for two one-slab-long, one-slab-wide modules joined side by side. (02-30-1093-3490Apb01)

cavity from solarization, and are filled with 200 Torr of Xe gas. The flash lamps were manufactured by EG&G, Inc. The 16 flash lamps in each central flash-lamp array are spaced 3.94 cm apart, corresponding to a lamp packing fraction (defined for central arrays as the bore diameter divided by the center-to-center distance) of 0.64. Like MSA-1 and MSA-2, silver diamond-shaped reflectors are placed between the lamps to increase efficiency.

The ten lamps in each side array are spaced 6.29 cm apart, corresponding to a lamp packing fraction (defined for side arrays as half the bore diameter divided by the center-to-center distance) of 0.79. As in MSA-2, a higher lamp packing fraction is used in the side arrays than in the central arrays to better balance pumping on the two sides of the laser slabs.

To further reduce costs, especially for the pulsed power system, only six flash lamps are installed in the side arrays on the inactive side (the side opposite the real Nd:Glass laser slabs) of the amplifiers. Experiments previously performed on MSA-1 showed that very little of the pump light produced by the flash lamps on the far side is transmitted by the central flash-lamp array under normal operating conditions.

Inspections show that after nearly one year of operation the Beamlet flash lamps remain essentially free of the C "brown spots" that commonly appear on Nova lamps. The improved cleanliness is partly attributed to the use of O-ring seals on the lamp bases that protect the lamp envelopes from outside sources of contamination.

During the amplifier activation tests, which were conducted when the Beamlet cavity amplifier was one, two, and five slabs long, the ends of the amplifiers were covered with hard-anodized panels. These panels kept the amplifiers clean and absorbed flash-lamp light. The panels had adjustable slits permitting gain measurements at any location in the amplifier aperture. To reduce the risk of contaminating the laser slabs, either with particles from the laser bay or particles that might have been generated when the panels were moved, each end panel was separated from the amplifier by an empty BAU.

Pulsed Power Description

The Beamlet pulsed-power system is described more fully in "Beamlet Pulsed-Power System" on p. 62 of this *Quarterly*. In brief, we use single-mesh LC circuits (circuits with inductance and capacitance) to drive pairs of flash lamps connected together in series. Each circuit has a 208-μF capacitor and a 140-μH inductor, and the $3(LC)^{1/2}$ pulse length is 500 μs. The measured capacitor-to-lamp transfer efficiency is 71%. To improve pumping efficiency, the flash lamps are preionized with 0.2-J/cm^2 pulses (electrical energy per unit of bore area) delivered 200 μs before the main pulses.[7,8]

The flash-lamp pulse energies, expressed in explosion fraction units, range from 0.075 to 0.30. Flash-lamp explosion fraction, f_x, is defined as the total electrical energy delivered to a flash lamp divided by the electrical energy required to explode the flash lamp on a single shot. Using the standard formula,[9] the single-shot explosion energy for the Beamlet flash lamps is 60.0 kJ per lamp.

Amplifier Gain Characterization Method

An important parameter in amplifier design is the gain of the amplifier. In this section, we describe the experimental layout to characterize gain, and how the gain measured on a one-slab-long amplifier may be used to obtain the gain for a chain of amplifiers.

13-Beam Gain Probe

To measure gain distributions over the entire aperture width on a single shot, we generated thirteen 5-mm-diam probe beams using beam splitters, rattle optics, and an 8-W continuous-wave (cw) Nd:YLF laser. The probe beams, which measure gain distribution by tracking changes in their own intensity, were centered in the aperture horizontally. The beam-to-beam spacing was 3 cm except for the two probe beams nearest the middle, where the spacing was 6 cm. To measure gain distributions over the entire aperture, the probe beams were moved to different vertical locations using a motor-driven stage to translate a turning mirror.

After passing through the amplifier, the probe beams struck an array of 13 PIN-44 photodiodes. To reduce the sensitivity of the gain measurements to lateral translations of the probe beam, we illuminated the photodiodes indirectly, using cavities made of diffusely reflecting material. Background flash-lamp radiation was reduced by the use of narrow-band interference filters and by placing the photodiodes 4–5 m away from the amplifiers. Neutral-density filters protected the photodiodes from saturation. The remaining flash-lamp contributions were eliminated by subtracting the signal produced by a 14th diode, which was physically close to the other diodes but had no incident probe beam. Scale factors for the subtracted signals, which were different for each channel, were obtained by firing the amplifiers with the probe beams turned off.

The photodiode signals were digitized at 0.5 MHz with 10-bit resolution. The shot-to-shot variations in the measured gain coefficients were about ±1%.

Predicting Amplifier Performance

The symmetry of the Beamlet (and NIF) amplifiers leads to a simplified method for predicting their performance. Figure 4 illustrates this method schematically. Here an amplifier N slabs long (in this case $N = 7$) is displayed in plan view [Fig. 4(a)]. Because of the system symmetry it can be shown[6] that the gain for an N-slab-long amplifier is a linear combination of three simple amplifier pump configurations: "X," "V" and "diamond" [Fig. 4(b)]. This observation greatly simplifies the testing needed to predict the performance of a Beamlet or NIF MSA consisting of an arbitrary number of slabs. Rather than having to build the complete N-slab-long amplifier, we can simply test one- and two-slab-long modules and extrapolate the performance of the N-slab-long unit. Note that if a mirror is placed on one end of a V configuration module, a diamond is formed, and if the mirror is placed on the other end of a V configuration module, an X is formed [see Fig. 4(b)]. Thus, by using a flat silver reflector at the end of the one-slab long module, one can also simulate the diamond and X pump configurations without having to build separate two-slab-long test modules [Fig. 4(b)]. This is the approach we have used successfully on Beamlet and will also use for the NIF amplifier development.

The basic assumption in this method is that the main pumping contributions are additive.[6] This assumption leads to an expression for α_i, the gain coefficient for an internal slab that is a function of gain measured in the three test configurations:

$$\alpha_i = \alpha_d + \alpha_x - \alpha_v \quad , \tag{3}$$

where α_d, α_x, and α_v are the gain coefficients measured in the diamond, X and V configurations, respectively. Similarly, α_N, the average gain coefficient for an amplifier N slabs long (where N is odd), is given by

$$\alpha_N = \frac{\left[\alpha_x + \alpha_d + (N-2)\alpha_i\right]}{N} \quad . \tag{4}$$

Generally, an odd N is desired to achieve good gain uniformity. This is because of gain gradients in the two end slabs. These gradients can be rather large and are caused by the loss of pump light out the ends of the cavity. By using an odd number of slabs, the gradients can be made to run in opposite directions and therefore tend to cancel each other out.

To test the above extrapolation technique for predicting amplifier performance, we compared measured and predicted gain distributions for a five-slab-long Beamlet amplifier. The gain measurements were made

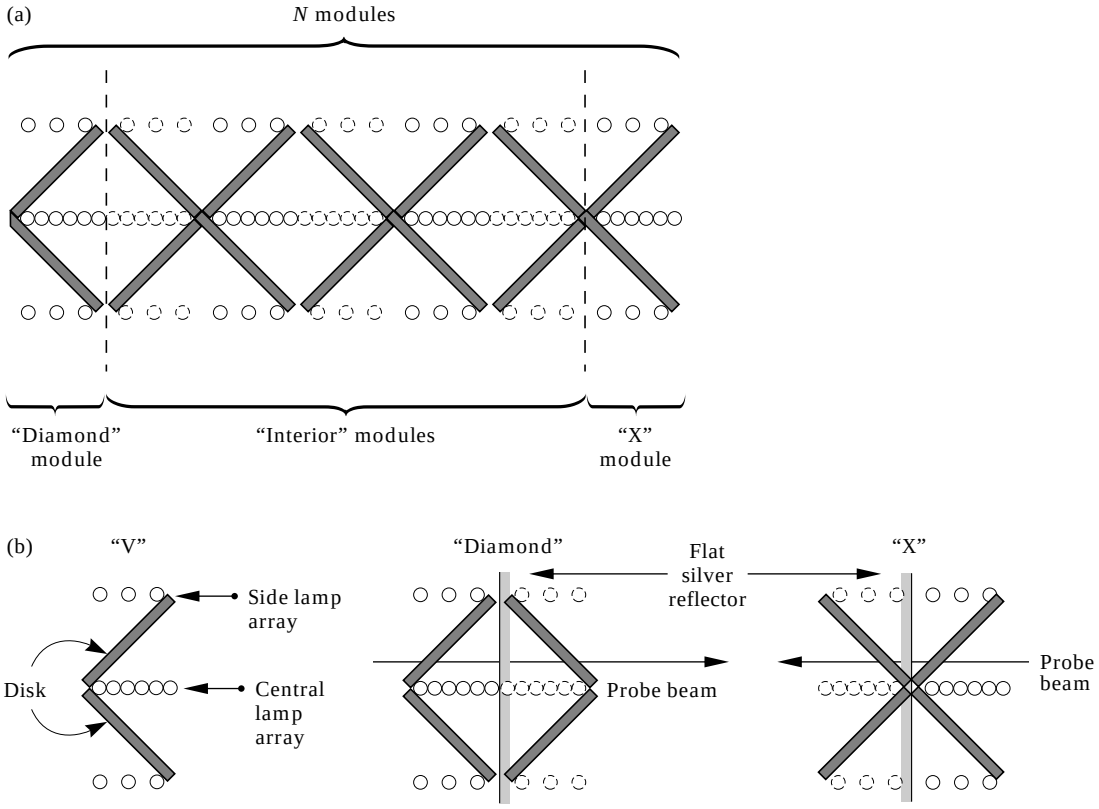

FIGURE 4. (a) Schematic drawing of an N-slab-long amplifier. (b) The three simple amplifier modules (X, V, and diamond) that were tested and used to predict the performance of the N-slab-long amplifier. (70-50-1294-3979pb01)

horizontally across the aperture and at the vertical middle using five different lamp explosion fractions ranging from 0.075–0.25. Figure 5(a) shows the horizontal gain distributions measured at $f_x = 0.2$ for the diamond, X, and V test configurations. From these measurements, we predicted the gain performance of a five-slab-long Beamlet amplifier and then compared it with actual measurements, shown in Fig. 5(b). The predicted and measured gain distributions for the five-slab-long amplifier have about the same shape, but the predicted value is about 5% higher. This discrepancy is because the predicted gain—Eq. (3)—does not take into account the nonlinear effect ASE has on the gain distribution. The slabs interior to the amplifier have higher gain coefficients, and therefore higher ASE decay rates, than the slabs in the X, V, and diamond configurations. For the NIF amplifier development, these and other results taken at different lamp explosion fractions will be used to validate an improved technique for predicting amplifier performance that takes ASE into account.

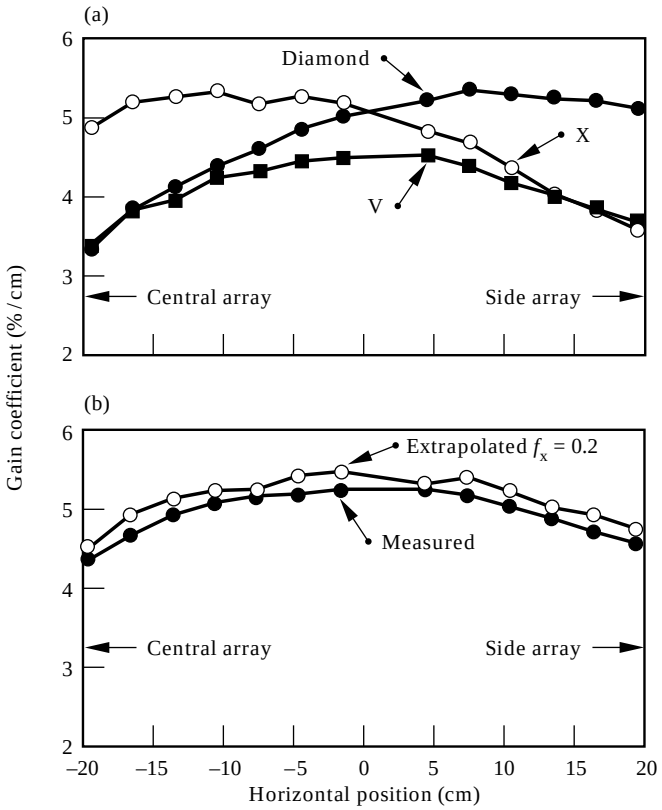

FIGURE 5. Horizontal gain distributions for (a) the V, diamond and X amplifier test configurations, and (b) the five-slab-long Beamlet amplifiers at $f_x = 0.20$. For comparison the predicted "extrapolated" performance for the five-slab-long Beamlet amplifier is also shown. (70-50-1294-3978pb01)

The gain coefficient profiles in Fig. 5(a) illustrate two other points about the amplifiers. First, note that the slopes in the gain distributions of the two slabs in the X and diamond configurations do not cancel out, because they have an even number of slabs (i.e., 2). Second, the one-slab-long amplifier (V) has a gain distribution similar to that of the five-slab-long amplifier (because N is odd), but the gain for the V is much lower due to large end-loss effects. The end losses also cause the two-slab-long amplifiers to have a lower average gain than the five-slab-long case.

Beamlet Amplifier Characterization Measurements

In addition to the gain, the storage efficiency and pump balance are important amplifier parameters. In this section, we discuss the results of our gain measurements and how they may be used to compute storage efficiency and pump balance.

Horizontal Gain Distributions vs f_x

Figure 6 shows horizontal gain distributions for the five-slab-long amplifier, which were measured at six different values of f_x. These gain distributions are relatively flat at low f_x and become more peaked as f_x increases. We attribute the higher gain at the center of the aperture to two effects: (1) ASE, which preferentially depumps the edges of the aperture and becomes more important as the average gain coefficient in the slab is increased; and (2) changes in the pump distribution as

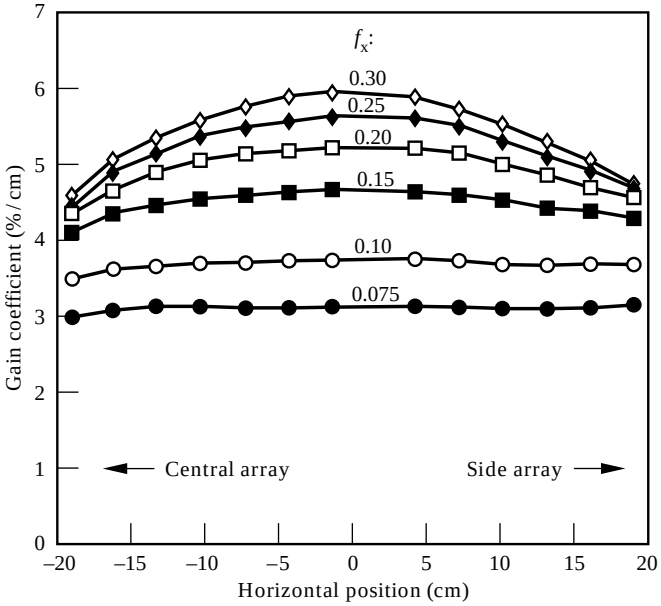

FIGURE 6. Horizontal gain distributions measured on the five-slab-long Beamlet amplifier at six different flash-lamp explosion fractions. (70-50-0494-2129pb01)

energy to the flash lamps is changed. It appears that ASE is the stronger of the two effects, based on MSA-2 experiments that showed that pump distributions produced by similar flash-lamp arrays varied only slightly with changes in how hard the lamps are driven (i.e., f_x).

Temporal Variations in the Horizontal Gain Distributions

Figure 7(a) shows the horizontal gain distributions that were measured on the five-slab-long amplifier at different times after initiation of the main pump pulse. In the figure, time increases from bottom to top for the rising edge of the pulse, and from top to bottom for the falling edge. The times were chosen to facilitate comparisons between gain distributions measured on the rise and fall of the gain, at comparable values of the average gain coefficient, as may be seen in Fig. 7(b). The gain distributions measured at the peak and on the fall of the pump pulse show the gain-peaking near the middle of the aperture that is attributed to ASE. The gain distributions measured on the rise lack this peaking effect, but show other types of variations that are attributed to nonuniform pumping. It appears that the pump distribution is not as uniform early in the pulse as it is later, after the arcs in the flash lamps have become better developed. These curves are indicative of the complexity that must be included in ray-trace codes to accurately predict gain distributions, as well as the wealth of Beamlet amplifier data now available for rigorous validation of such codes.

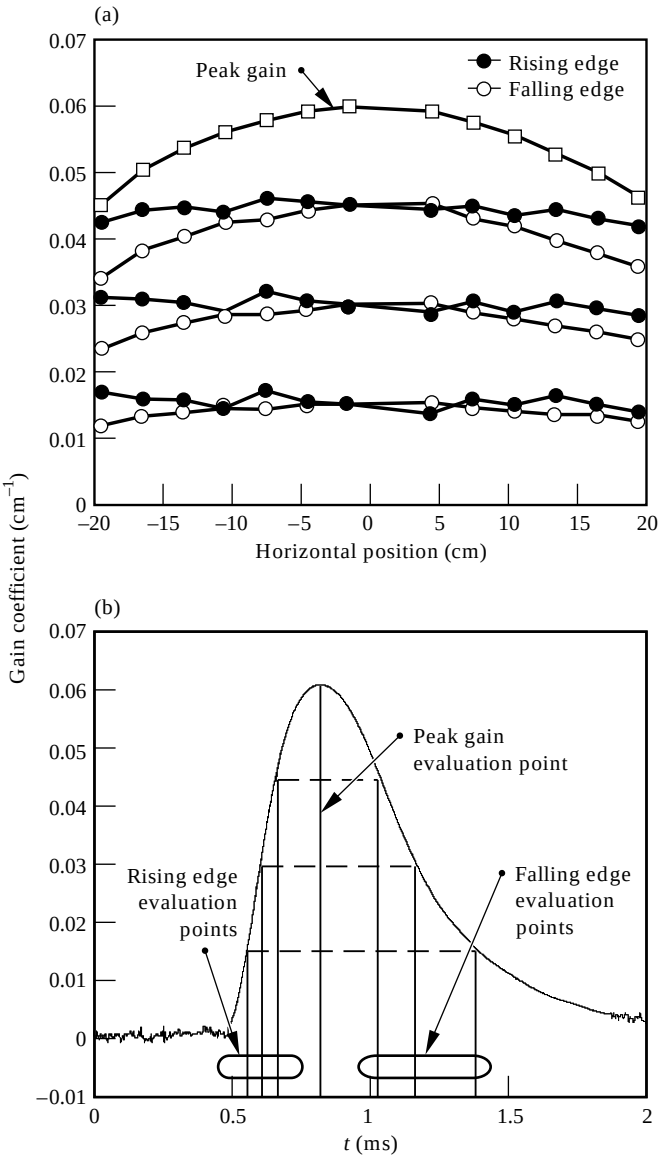

FIGURE 7. (a) Horizontal gain distributions of the five-slab-long Beamlet amplifier at different times during the main flash-lamp pulse, shown vs time in (b). (70-50-1294-3977pb01)

Full-Aperture Gain Distributions

Knowledge of the gain distribution over the full aperture is also required for rigorous validation of amplifier performance models. Full-aperture gain distributions were measured for the diamond, X, and five-slab-long amplifiers, at flash-lamp explosion fractions of 0.15 and 0.20. Figure 8 shows a contour plot of the full-aperture gain distribution measured on the five-slab-long amplifier at f_x = 0.20. Except for regions near the top and bottom of the aperture where the slab is partially shadowed by its mask, the gain gradients were larger in the horizontal direction than in the vertical direction because of ASE. For this gain distribution, in the central 95% of the aperture, the

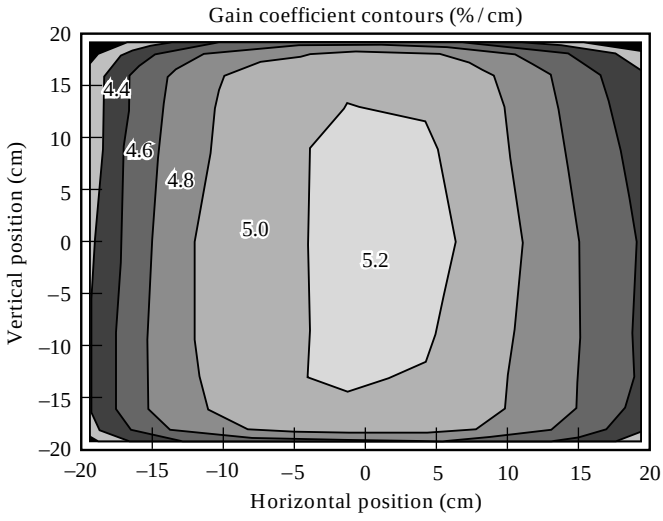

FIGURE 8. Gain distribution across the aperture of the five-slab-long Beamlet amplifier. (02-30-1093-3495pb01)

peak-to-average ratio of the gain coefficient *(U)* was 1.06 ± 0.004. In comparison, the MSA-2 amplifier, which had a similar pump cavity design, attained a *U* value of 1.025 ± 0.004. We attribute most of this difference to the higher ASE rates because of the Beamlet amplifier's larger pumped aperture (39.5×39.5 cm^2 compared to 29×29 cm^2 for MSA-2).

Storage Efficiency

Figure 9 shows storage efficiency vs gain per slab for the five-slab-long Beamlet amplifier and the Nova 31.5- and 46-cm amplifiers. At f_x = 0.20, the normal operating point for all three amplifiers, the Beamlet amplifier has a storage efficiency of 3.0%, compared to 1.8% for the Nova amplifiers. The principal factors causing the Beamlet amplifiers to attain higher storage efficiency are lower lamp packing fraction, shorter flash-lamp pulse length, and the use of more efficient central flash-lamp arrays in the 2×2 MSA architecture. Because of the large size of the Beamlet slabs and higher ASE decay rates, the efficiency curve for the Beamlet amplifier decreases faster than for the Nova amplifiers as gain per slab increases.

Pump Balance

Balanced pumping helps to reduce pump-induced beam steering. To determine how well balanced the pumping is between the central and side flash-lamp arrays, we measured horizontal gain distributions in the two-slab-long amplifiers while firing the central and side flash-lamp arrays separately. End losses were minimized by firing the central flash-lamp array in the diamond configuration and by firing the side flash-lamp array in the X configuration. Figure 10 shows the average gain coefficient plotted vs flash-lamp explosion fraction, for both central- and side-array pumping. We calculated average gain coefficients by integrating the measured horizontal gain distribution across the aperture. We found that over the entire explosion fraction range, from f_x = 0.075–0.25, pumping by the two flash-lamp arrays was balanced to within 5%, with the central array achieving slightly higher average gain coefficients than the side array.

Pump-Induced Wavefront Distortion

In the MSA geometry, the front and back of the laser slab gets heated unequally by the pump radiation. As a result, thermal stresses build up and cause the slab to deform. This deformation results in wavefront distortion of an initially plane beam. In this section, we describe our work in measuring pump-induced wavefront distortion.

Local Beam-Steering Probe

During the Beamlet amplifier activation, we characterized pump-induced wavefront distortion in the Beamlet amplifiers by measuring local pump-induced beam-steering angles using three 5-mm probe beams, generated with the cw Nd:YLF laser described earlier.

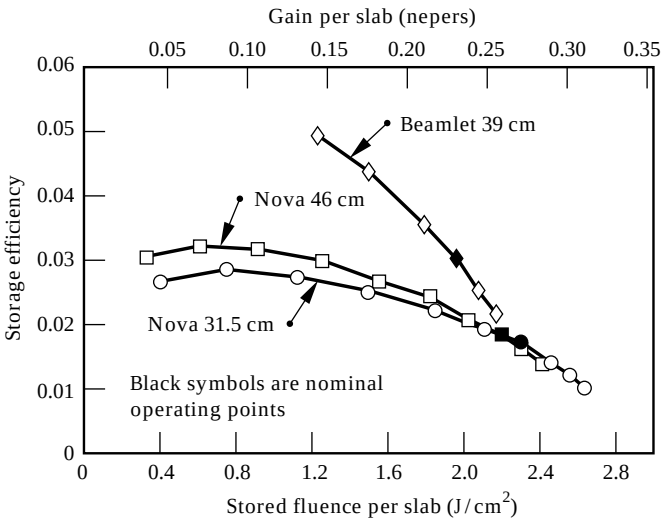

FIGURE 9. Storage efficiency vs the small signal gain per slab (and stored fluence per slab) for the five-slab-long Beamlet amplifier and the Nova 31.5-cm and 46-cm amplifiers. (70-50-0494-19589pb01)

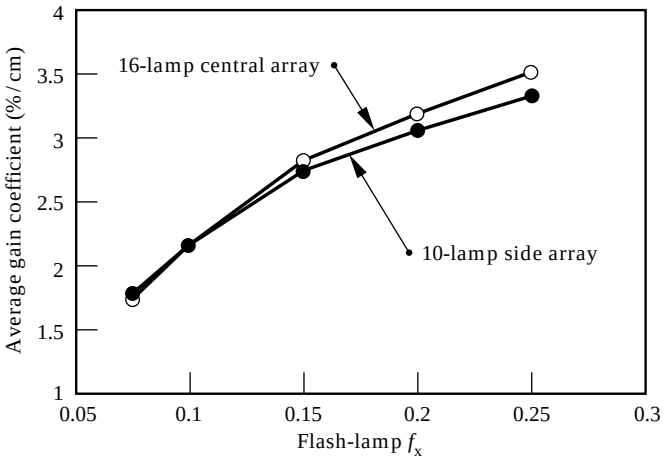

FIGURE 10. Average gain coefficient vs flash-lamp explosion fraction for two cases: (1) only the central array was fired (in the diamond configuration); and (2) only one of the side arrays was fired (in the X configuration). Central and side pumping were balanced over a wide range of explosion fractions. (70-50-1294-4015pb01)

The wavefront distortion in waves, Φ, is related to the local beam-steering angle, $\Delta\Theta$, by

$$\Phi(x) = \frac{1}{\lambda_0}\int_0^x \Delta\Theta(x')\,dx' \quad , \tag{5}$$

where x and x' are positions in the aperture and λ_0 is the wavelength. The three probe beams were arranged in a column, with a 9-cm vertical separation between adjacent probe beams. A motor-driven stage was used to move the three probe beams to different aperture positions.

The method for measuring local beam-steering angles has been described previously.[10] After passing through the amplifier, each probe beam was split, with one part directed to a lateral-effect photodiode and the other part to a conventional photodiode. Lateral-effect photodiodes produce output voltages proportional to the product of the beam power and the displacement of the beam centroid from the center of the detector. Each lateral-effect photodiode was placed at the focus of a 2-m-focal-length lens to ensure that the output voltages were proportional to changes in the propagation direction of the probe beam, and were insensitive to lateral translations of the probe beams. The lateral-effect photodiodes produced two beam-steering signals, one for the horizontal direction and one for the vertical direction. The effects of variations in probe beam power were removed by dividing the output voltages from each lateral-effect photodiode by the output voltage from the corresponding conventional photodiode. Integrating spheres ensured that the conventional photodiode signals were insensitive to lateral beam translations. The apparatus was calibrated absolutely by placing in each probe beam a rotating wedge with 208 μradian of angular deflection. Beam-steering and gain signals were digitized at a 200-kHz rate with 10-bit resolution.

The effects of static and quasi-static distortions were removed by subtracting the beam-steering angle measured during the pump pulse from the beam-steering angle measured 50–100 μs prior to the flash-lamp preionization pulse. The shot-to-shot variations in the beam-steering angles measured at the time of peak gain were approximately ±0.25 μradian. This reproducibility was achieved by placing the laser, amplifiers, and diagnostics under a class-100 HEPA filter hood to shield the beam paths from air turbulence. The blowers in the hood and the N_2 gas flow in the amplifiers were turned off during shots.

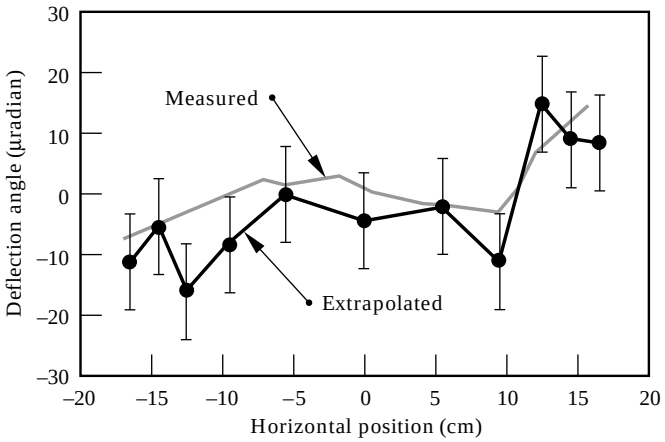

FIGURE 11. Pump-induced horizontal beam-steering angle vs horizontal position in the aperture for the four-pass 11-slab-long amplifier at f_x = 0.2. Values extrapolated from the diamond, X, and 5-slab-long amplifier data are in good agreement with values measured directly using a Hartmann sensor. (70-50-1294-3976pb01)

Results from Pump-Induced Distortion Measurements

We measured pump-induced beam-steering angles $\Delta\Theta_d$, $\Delta\Theta_x$, $\Delta\Theta_5$ on the diamond, X, and five-slab-long amplifiers, respectively. Using the formulas

$$\Delta\Theta_i = \frac{\left[\Delta\Theta_5 - \left(\Delta\Theta_d + \Delta\Theta_x\right)/2\right]}{3} \tag{6}$$

and

$$\Delta\Theta_{cav} = 4\left[9\Delta\Theta_i + \left(\Delta\Theta_d + \Delta\Theta_x\right)/2\right] \quad , \tag{7}$$

we obtained the pump-induced beam steering angles $\Delta\Theta_i$ for an interior slab and $\Delta\Theta_{cav}$ for a four-pass eleven-slab-long cavity amplifier, respectively. Figure 11 shows the pump-induced horizontal beam-steering angle vs horizontal position in the aperture for the four-pass eleven-slab-long amplifier, with the flash lamp fired at f_x = 0.2. Shown with our data are pump-induced beam-steering angles measured directly on the four-pass eleven-slab-long amplifier with a Hartmann sensor, as described in "Beamlet Pulse-Generation and Wavefront-Control System," p. 42. The beam-steering angles measured with the two techniques are in good agreement, with pump-induced beam-steering angles falling within ±15 μradian over most of the aperture. Negative angles correspond to beam steering toward the central flash-lamp arrays while positive angles correspond to beam steering toward the side flash-lamp arrays.

The pump-induced phase variation across the aperture, calculated using Eq. (5), was <2 waves at 1.053 um. With active wavefront correction using a deformable mirror, the phase variation was reduced to approximately 0.7 waves, well within Beamlet focusing and harmonic conversion requirements.

The major conclusions drawn from our beam-steering measurements are that in the central region of the slab more than one-half slab thickness from the edge claddings, pump-induced wavefront distortion is only weakly dependent on the vertical location in the aperture; pump-induced beam steering is much greater in the horizontal direction than in the vertical direction; and pump-induced beam steering is much greater in the end slabs than in the interior slabs. These results are consistent with previous pump-induced beam-steering measurements conducted at LLNL and with our understanding of pump-induced wavefront distortion. They are important because they confirm our understanding of the process and they establish confidence in our design of the NIF amplifiers.

Summary

We have completed detailed gain and pump-induced beam-steering measurements on the Beamlet amplifiers. The measurement results will be used to rigorously validate new and improved models for predicting amplifier performance, and will be of great value in the development of the NIF amplifiers. For the first time, MSA performance has been demonstrated at approximately the same aperture dimensions that are anticipated for the NIF.

Acknowledgments

The authors wish to thank Schott Glass Technologies[11] for providing lasers slabs, and EG&G, Inc.[12] for providing flash lamps, both critical parts of the work on Beamlet.

Notes and References

1. W. E. Martin, J. B. Trenholme, G. J. Linford, S. M. Yarema, and C. A Hurley, *IEEE J. Quantum Electron.* QE-9, 1744–1755 (1981).
2. H. T. Powell, A. C. Erlandson, K. S. Jancaitis, and J. E. Murray, *High-Power Solid State Lasers and Applications* (SPIE—The International Society for Optical Engineering, Bellingham, WA, 1988; *Proc. SPIE* 1277), pp. 103–120 (1990).
3. K. S. Jancaitis, private communication: ray-trace model.
4. M. D. Rotter, LLNL memorandum AMP 92-006.
5. W. F. Hagen, *Laser Program Annual Report, 1977*, 2-228 to 2-231, Lawrence Livermore National Laboratory, Livermore, CA, UCRL-50021-77 (1978).
6. A. C. Erlandson, K. S. Jancaitis, R. W. McCracken, and M. D. Rotter, *ICF Quarterly Report* 2(3), 105–114, Lawrence Livermore National Laboratory, Livermore, CA, UCRL-LR-105821-92-3 (1992).
7. J. E. Murray, *Laser Program Annual Report, 1985*, 7-3 to 7-13, Lawrence Livermore National Laboratory, Livermore, CA, UCRL-50021-85 (1986).
8. A. C. Erlandson, *Laser Program Annual Report, 1985*, 7-18 to 7-25, Lawrence Livermore National Laboratory, Livermore, CA, UCRL-50021-85 (1986).
9. J. H. Goncz, *ISA Transactions* 5, 28 (1966).
10. J. E. Murray, H. T. Powell, G. F. Ross, and J. D. Winemute, Technical Digest, Annual Meeting, *Opt Soc of Am*, Washington, DC, TUU9 (1988).
11. Schott Glass Technologies Inc., 400 York Ave., Duryea, PA, 18642.
12. EG&G, Inc., Electro-Optics Division, 35 Congress St., Salem, MA, 01970.